World Academy of Science, Engineering and Technology
International Journal of Aerospace and Mechanical Engineering
Vol:19, No:2, 2025

Design and Thermal Analysis of Power Harvesting System of a Hexagonal Shaped Small Spacecraft

Mansa Radhakrishnan, Anwar Ali, Muhammad Rizwan Mughal

***Abstract*—**Many universities around the world are working on modular and low budget architecture of small spacecraft to reduce the development cost of the overall system. This paper focuses on the design of a modular solar power harvesting system for a hexagonal-shaped small satellite. The designed solar power harvesting systems are composed of solar panels and power converter subsystems. The solar panel is composed of solar cells mounted on the external face of the printed circuit board (PCB), while the electronic components of power conversion are mounted on the interior side of the same PCB. The solar panel with dimensions 16.5 cm × 99 cm is composed of 36 solar cells (each solar cell is 4 cm × 7 cm) divided into four parallel banks where each bank consists of 9 solar cells. The output voltage of a single solar cell is 2.14V, and the combined output voltage of 9 series connected solar cells is around 19.3V. The output voltage of the solar panel is boosted to the satellite power distribution bus voltage level (28V) by a boost converter working on a constant voltage maximum power point tracking (MPPT) technique. The solar panel module is an eight-layer PCB having embedded coil in 4 internal layers. This coil is used to control the attitude of the spacecraft, which consumes power to generate a magnetic field and rotate the spacecraft. As power converter and distribution subsystem components are mounted on the PCB internal layer, therefore it is mandatory to do thermal analysis in order to ensure that the overall module temperature is within thermal safety limits. The main focus of the overall design is on compactness, miniaturization, and efficiency enhancement.

***Keywords*—**Small satellites, power subsystem, converter, maximum power point tracking, MPPT.

I. Introduction

THERE has been a significant transformation in space exploration and satellite technology in recent years, thanks to the emergence of small satellites, commonly known as "small sats" or "nanosatellites". These compact spacecrafts have become increasingly popular due to their affordability, adaptability, and ease of access. Small satellites are diminutive and lightweight spacecraft specifically engineered for a wide range of missions such as Earth observation, communication, scientific investigations, technology validation, and numerous other applications. These satellites are distinguished by their relatively modest dimensions, minimal mass, and streamlined construction that led to decreased launching costs and quicker development time as compared to conventional, larger satellites [1], [2].

Hexagonal prism-shaped spacecraft (Fig. 1) constitutes a unique category of small satellites celebrated for their uncommon geometric design. Frequently employed for missions with specific requirements, these spacecrafts combine structural efficiency with adaptability, contributing to the advancement of space exploration. Hexagonal prism-shaped spacecrafts, as their name implies, have a hexagonal cross-sectional structure characterized by six flat sides arranged in a hexagonal pattern. This distinctive geometric design distinguishes them from the more typical cubic or rectangular satellite shapes. The selection of this shape is motivated by several factors, including the need for structural robustness, payload capacity, and alignment with specific mission demands [3], [4]. To achieve their missions efficiently, hexagonal prism spacecraft rely on a range of subsystems. Solar panels capture solar energy for powering spacecraft systems [3], [5]. Communication subsystems transmit data to and from the spacecraft, while attitude control uses sensors and actuators [6], [7]. Thermal control uses insulation to protect the spacecraft from extreme temperatures [8], [9]. Data handling and processing subsystems manage tasks and store data [3]. Payload subsystems use optical payloads for scientific observations. Structural subsystems provide the spacecraft's structure. Command and data handling subsystems handle instructions from ground control and archive data [3]. Telemetry and tracking subsystems relay information about the spacecraft's health and status to ground control [7], [10].

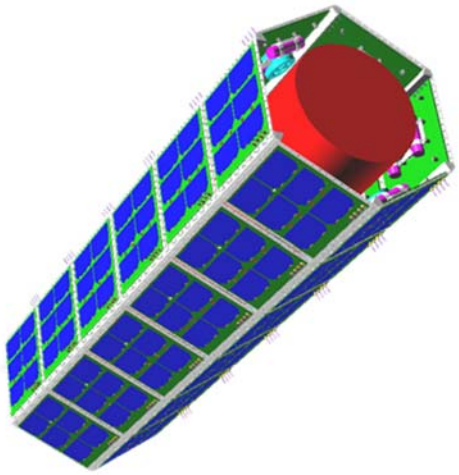

Fig. 1 Hexagonal Shaped Small Satellite

II. Power Subsystem

In recent years, there has been a growing interest among

Mansa Radhakrishnan and Anwar Ali* are with Electronics and Electrical Engineering Department, Swansea University, Bay Campus United Kingdom (*corresponding author, e-mail: anwar.ali@swansea.ac.uk).

Muhammad Rizwan Mughal is with Department of Electrical and Computer Engineering, Sultan Qaboos University (SQU), Muscat, Oman.

researchers in creating CubeSats, which are designed to carry compact payloads for straightforward missions in the low Earth orbit (LEO). The various components aboard the CubeSat require a consistent supply of electrical power. Therefore, there is a necessity for a dependable power system that can effectively fulfil the requirement of providing the necessary electrical power to each subsystem. The Electrical Power System (EPS) is designed to deliver electrical power to the CubeSat. This entails continuous power generation to sustain the satellite's operations, power storage through batteries to support the CubeSat during periods when primary power generation is unavailable, monitoring the power to be distributed, and safeguarding the CubeSat's circuits in the event of a malfunction or fault [11]. Because they depend on solar panels for power, CubeSats are limited in power even if they are small and light. This is especially important when there is an eclipse [12], [13]. Due to their small size, CubeSats are not as equipped with sensors, instruments, or equipment, which restricts their mission range and ability to collect data [14]. Furthermore, maintaining ideal thermal conditions is essential to the functionality of onboard systems [15].

Using a hexagonal-shaped satellite can overcome all these drawbacks of CubeSat. Following are some of the advantages of the hexagonal shaped spacecraft:

- *Special Shape:* Hexagonal satellites look different from the usual cube shaped CubeSats. This unique shape can be beneficial because it helps with fitting equipment, and deciding where to put propulsion systems, and might even make it work better in space.
- *Flexible Payload:* The hexagonal shape allows for more freedom in arranging and putting together the equipment (payloads and instruments) inside the satellite. This means we can use larger or more complicated gear for the mission.
- *Efficient Solar Panels:* Hexagonal satellites are skilled at placing solar panels in the best spots to capture lots of sunlight and make a lot of electrical power. This is especially handy for missions that need a lot of power to run their systems.

The EPS is undoubtedly one of the spacecraft's most vital components. Its primary role is to guarantee the dependable provision of electrical power that is compatible with all mission phase requirements and can accommodate all loads. It includes a solar cell array, DC/DC converters, battery charge/discharge controller, power control distribution unit and load [16], [17].

A. Solar Cell

Multi-junction solar cells are currently the most efficient photovoltaic technology available. These cells primarily utilize III-V semiconductors known for their superior radiation resistance, making them highly appealing for use in space applications. Furthermore, their minimal sensitivity to temperature changes translates to improved performance in the extreme operating conditions experienced in outer space [18].

For this paper, a Triple Junction GaAs Solar Cell is used. These solar cells are a variant of multi-junction solar cells featuring three distinct semiconductor layers, or junctions, arranged in a stack [19]. Each junction is precisely configured to absorb specific wavelengths of light. This unique design enables triple-junction cells to attain increased efficiency by capturing a wider spectrum of solar radiation. Their exceptional performance in low-light situations makes them particularly suitable for space missions, including those conducted in deep space or under conditions with restricted sunlight. Some of the standard sizes of these cells are 6.9 x 3.9 cm^2, area 26.5 cm^2; 4 x 8 cm^2, area 30.15 cm^2 (also available: 7.6 x 3.7 cm^2, area 27.5 cm^2; 6 x 12 cm^2; area 68.6 cm^2) [19].

Fig. 2 Image of a CTJ30-80 solar cell in a curved arrangement [19]

CESI has created exclusive triple-junction space solar cells, known as CTJ30-80, with an 80-micrometer thickness and a unique epitaxial structure comprising InGaP/InGaAs/Ge. These solar cell structures were cultivated on 100 mm diameter Ge substrates, initially measuring 140 micrometres in thickness. After the epitaxial growth phase, a wet etching technique was applied to thin the Ge substrate down to 80 micrometres. These carefully chosen conditions allowed to production of thin, consistently thick substrates without compromising the electrical performance in comparison to conventional 140 µm thick solar cells. Each wafer yielded two solar cells, each with dimensions of 26.5 cm^2 and an average mass of 1.3 grams. Both the front and rear contacts were formed using a 5 micrometre-thick layer of evaporated silver, subsequently capped with a 200 nanometre-thick layer of gold [20].

B. Boost Converter

A boost converter is a type of switching converter that functions by intermittently turning an electronic switch on and off. It earns its name, "boost converter," because it results in an output voltage that is higher than the input voltage. DC converters play a pivotal role in all electronic designs as they manage voltage regulation and distribution based on the specific needs of the system, depending on its application. They aim to optimize the EPS stages, particularly by enhancing the charging process of solar panels and batteries. DC converters utilize techniques like pulse width modulation and feedback control to precisely regulate their output voltage, resulting in minimized losses and improved efficiency compared to linear regulators. These converters typically employ simple circuit topologies with few components, making them particularly well-suited for use in system-on-chip environments. In the context of battery charging, DC converters are evaluated as part of an architecture to ensure the highest possible efficiency,

ultimately maximizing energy collection. This efficiency is closely tied to the reduction of losses during conduction and commutation [21].

C. MPPT

MPPT, also known as Maximum Power Point Tracking, is a method used in power systems to enhance the efficiency of solar panel power collection. The main goal of MPPT is to guarantee that solar panels consistently operate at their maximum power point, where they can generate electrical energy from the available sunlight. Solar panels have a voltage-current characteristic that varies with changing sunlight conditions. The maximum power point (MPP) on this characteristic curve represents the point at which the panel generates the highest amount of power for a given level of sunlight. MPPT technique is used to monitor the solar panel voltage and regulates the output voltage and current, to ensure that the panels are operating at its MPP [22]. This is achieved by specialized electronics, typically in the form of an MPPT charge controller or inverter.

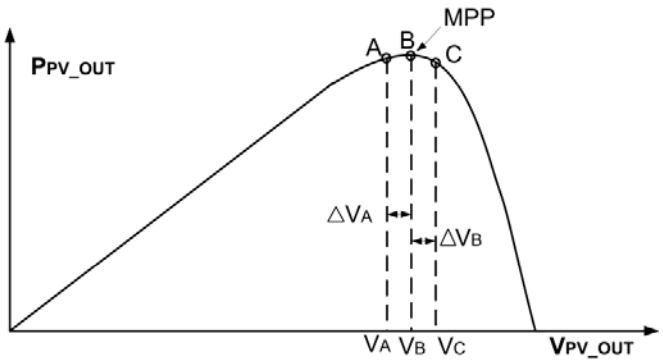

Fig. 3 Operation of the MPPT algorithm

As shown in Fig. 3, with an increase in the voltage (ΔV), there is a subsequent change in the output power (ΔP). Until point B, there is a steady rise in the graph. After that point, upon increasing the voltage, the power decreases. Hence the operating point should be continuously shifting between A, B, and C during typical MPPT at steady state. This means that the PV array voltage will continually fluctuate about the MPP voltage point using the MPPT method by constantly changing the PV array output voltage by a predetermined step (ΔV).

III. Proposed Method

The main components of a power subsystem – Solar Panel and Boost Converter with MPPT was designed.

A. Design of Solar Panel

One solar cell can give the output of 2.14V and 400mA. In this project, there are 9 cells connected in series to get nearly 19 voltages in output, and 4 combinations of solar cells connected in series to increase the current capacity to 1.6A output. Therefore, there are 36 solar cells placed in one panel. One diode is placed parallel to the solar cell to prevent the solar cell from the reverse voltage. One diode is connected in series with one solar row to stop the current flow within the solar rows itself. The diode used in this project is UPR10E3CT which comes in the SMD package. The second step is to make a PCB design followed by PCB libraries for the solar cell and the diode. As the design of the solar cell and diode is unique, it needs to be done in a separate PCB library.

There are different connections of solar cells in the solar panel to choose from like – 18 x 2, 2 x 18, 12 x 3, 3 x 12, 4 x 9 and 9 x 4. The connection must be chosen according to the output voltage and current requirements. For this project, the output voltage requirement is 19V and the output current requirement is 1.6A. One solar cell (CTJ30) generates 2.14V and 400mA of current. The total number of cells that fit into the solar panel is 36. Therefore, the solar cell connection must be made in such a way that it can give an output of 19V and 1.6A.

The most suitable arrangement was 9 x 4. In this combination, nine solar cells are connected in series. A total of four numbers of the same combinations are connected in parallel. Output voltage, V_o can be determined by multiplying number of cells in series with voltage per cell and output current, I_o can be found by multiplying number of cells in parallel with current per cell.

- Output Voltage, $V_o = 9 * 2.14 = 19.26V$
- Output Current, $I_o = 4 * 0.4 = 1.6A$

This combination has nearly 19V and 1.6A current, therefore, this combination is perfectly suitable.

B. Design of Boost Converter

The power subsystem module plays a crucial role in hexagonal satellites, comprising two primary sections: one for attitude sensors and the other for supplying electrical power to the satellite. A key component within the power subsystem is the boost converter, which serves the critical function of transforming the 19.26V output generated by a solar panel into a 28V output which feeds into the satellite's power supply bus. It typically consists of a minimum of two semiconductor switches (comprising a diode and a transistor) as well as at least one energy storage component (typically an inductor). To minimize voltage fluctuations in the input and output, capacitor filters are commonly incorporated at both ends of the converter. The MATLAB simulation circuit diagram of the boost converter for the power subsystem module is shown in Fig. 4.

The values of capacitance and inductance were found using the following equations [23]:

$$L = \frac{V_s DT}{\Delta i_L} = \frac{V_s D}{\Delta i_L f} \quad (1)$$

$$C = \frac{D}{R(\Delta V_o / V_o) f} \quad (2)$$

With an input voltage of 19V, output voltage of 28V, output resistance of 25Ω, frequency of 25 kHz and duty cycle of 0.3, 1% ripple, the calculated value of capacitance in boost converter was 1.344 mF. Similarly, the value of inductance is 72μH.

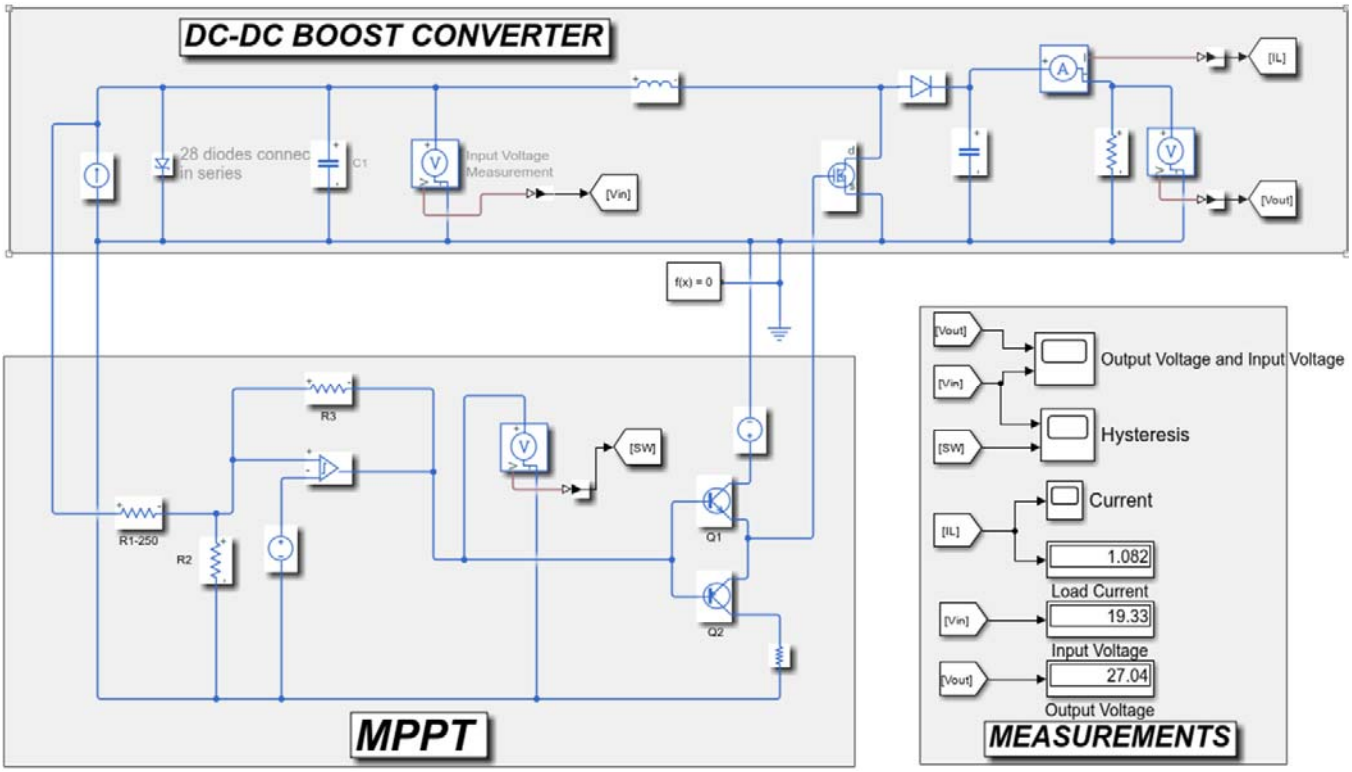

Fig. 4 MATLAB Simulation of Boost Converter for Small Satellite Power Subsystem

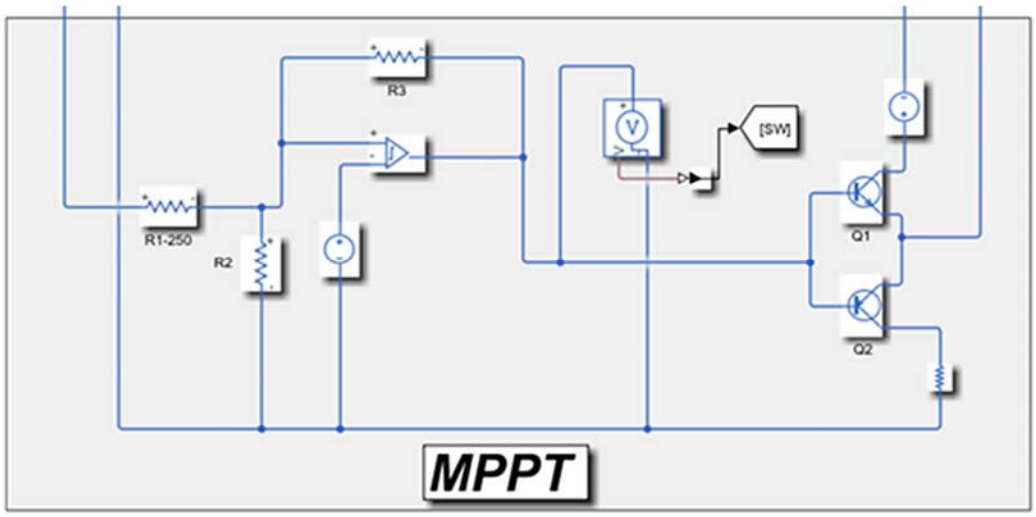

Fig. 5 Hysteresis Loop Comparator

C. Design of Maximum Power Point Tracker

A solar cell's performance can also be defined by its MPP, which occurs when the product $V_{mp} \times I_{mp}$ reaches its highest value Graphically, the maximum power output of a cell is represented by the largest rectangle that can fit under the I-V curve. To ensure that our boost circuit operates at the MPP, thereby extracting the maximum power from the solar cells, we run a boost converter in such a way that the power generated will oscillate around a MPP in a graph.

To ensure that our boost converter consistently operates at the MPP of the solar panel, we make use of the hysteresis loop within the comparator. It is worth noting that most comparators come with built-in hysteresis, typically in the range of 5 mV to 10 mV. This internal hysteresis serves the purpose of preventing the comparator from oscillating due to small parasitic feedback. However, when faced with external noise of greater magnitude, this internal hysteresis might not suffice. In such instances, we can enhance the performance by introducing external hysteresis. In our case, we incorporate approximately 1000 mV of hysteresis into our comparator, which is illustrated in Fig. 5.

Fig. 5 illustrates a hysteric comparator. The incoming voltage, derived from the variable solar panel output, is adjusted

using a resistive divider network and is then directed to the non-inverting input of the comparator. When this input voltage reaches 19.5V, surpassing the reference voltage (V_{ref} = 19V), the comparator's output goes high, activating the transistor. Subsequently, the voltage across the input filter capacitor $C1$ decreases, leading to a reduction in the input voltage of the comparator. However, the comparator maintains its output in the high state until the input voltage falls below 19V. Once the input dips below 19V, the comparator's output goes low, deactivating the switching transistor. This range between the lower limit (18.5V) and upper limit (19.5V) of these two voltages is referred to as the hysteresis window. To determine the values of the resistive network components R_1, R_2, and R_3 in Fig. 6, we started by specifying a hysteresis window band, which ranges from 18.5V to 19.5V, amounting to 1000 mV. Additionally, we set V_{CC} to 50V. As a first step, we chose a value for R_3, opting for a value of 25kΩ in our case.

$$R_1 = R_3\left(\frac{V_{HB}}{V_{CC}}\right) \tag{3}$$

To determine the V_{ref} value, we employ (4). By substituting all the known values into this equation, we can derive the V_{ref} value.

$$V_H > V_{ref}\left(1 + \frac{V_{HB}}{V_{CC}}\right) \tag{4}$$

We found V_{ref} <= 19, and we fixed it to 19V.

$$R_2 = {}^{1}\Big/\left[\left(\frac{V_H}{V_{ref} * R_1}\right) - \left(\frac{1}{R_1}\right)\right] - \left(\frac{1}{R_3}\right) \tag{5}$$

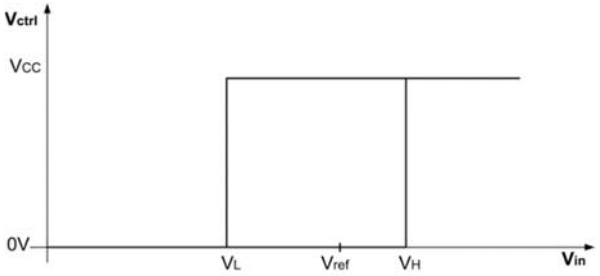

Fig. 6 Hysteresis Window for the Hysteresis loop comparator

To ascertain the value of resistor R_2, we can insert the known values of the various components into (5).

With the following values for Upper limit of voltage, V_H = 19.5V, Lower limit of voltage, V_L = 18.5V, Hysteresis Band voltage, V_{HB} = 1V, Reference voltage, V_{ref} = 19 and Resistance, R_3 = 25000Ω, the values of R_1 and R_2 are 500Ω and 79.2Ω respectively.

IV. Results and Analysis

A. Solar Panel Design

1) Schematic Design

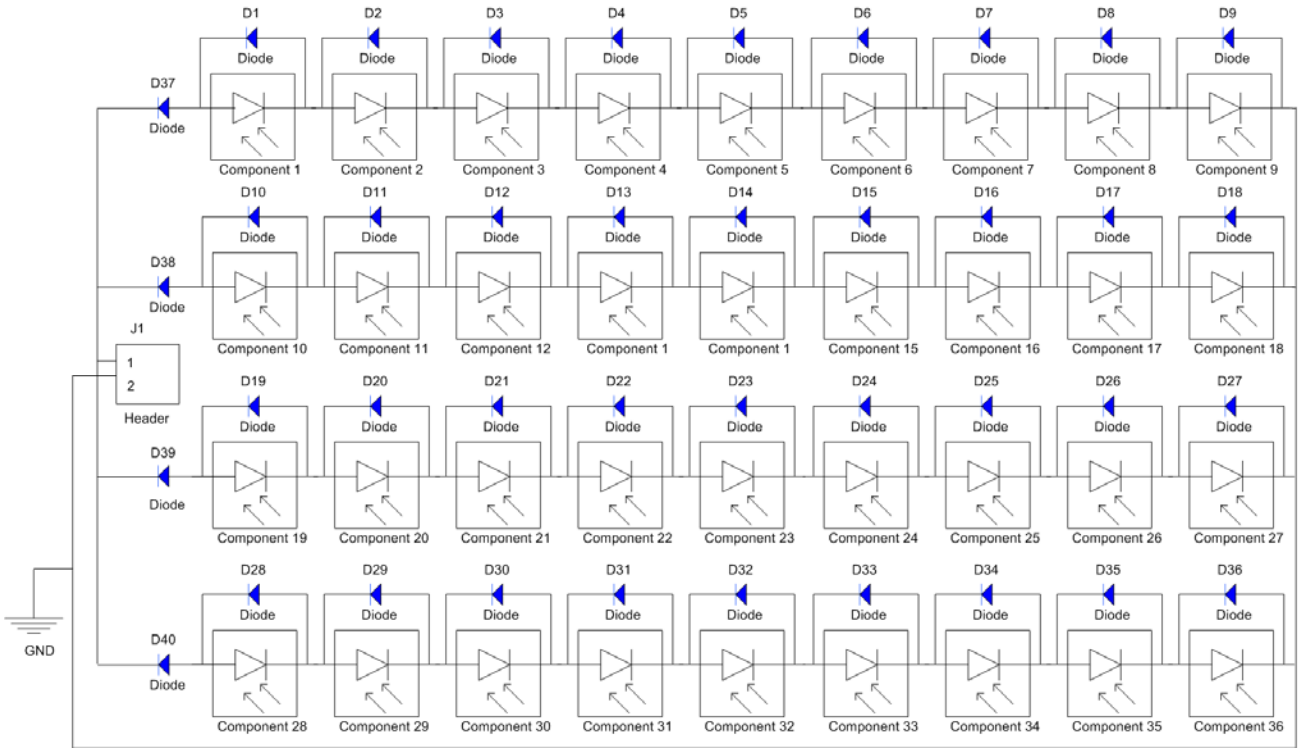

Fig. 7 Schematic diagram of the solar panel

The final schematic diagram is shown in Fig. 7. As discussed in various connections of solar cell, the last connection of 4 X 9 (9 in series, 4 in parallel), turned out as suitable connection for one solar panel. In one solar panel there are 36 cells in which

9 cells are connected in series in one row. There are 4 rows made of the same 9 cells in series. Finally, those four-cell arrays are connected in parallel to increase the current capacity. One antiparallel diode is connected in front of a solar cell to bypass the reverse voltage in case of fault.

In the same way, one UPR10E3 diode is connected in series with the solar cell array for the protection of a solar cell array. This diode will be in reverse bias when reverse voltage is applied. There are just two terminals of a solar cell that is taken out of a panel. Positive supply is connected to the positive bus of an array and negative terminal is connected to the ground bus of a solar panel.

2) PCB Design

- *Board Planning:* To carry out board designing, it is essential to set the board size. The board shape is drawn the same as the panel size. Solar panel board size is 990 mm X 165 mm which is shown in Fig. 8.
- *Design Rule Modification:* Frequently, in Altium Designer, designers inadvertently breach several common design rules due to oversights or human errors. These rule violations can lead to several issues, encompassing design problems, manufacturing complications, or electrical malfunctions in your PCB. The unique design of this panel causes many violations such as clearance, Track width standard, Plane clearance directives etc. However, these rules are redefined to incorporate with these rule violations.
- *Layer Selection:* Layer selection is an obvious decision to make. The top layer is mostly occupied by solar cells and diodes. Therefore, there is no space available to make the ground connection, so it is necessary to choose another layer as well. The top layer is indicated by red color and the bottom layer is indicated by blue color. It is clearly visible in Fig. 8 that the blue color indicates the second layer which is mostly designated to negative terminal connection.

B. Boost Converter with MPPT Using MATLAB

1) Input and Output Voltages

Input voltage is obtained from the solar panel which is approximately 19V. The output voltage supposed to receive is around 28V. It is clearly visible in Fig. 9 that the output voltage is boosted from 19V to nearly 28V. Output voltage is a little bit less than expected because of parasitic resistance and losses in the passive components. Moreover, to make the output precise, the close loop control can be introduced to get precise output voltage.

From Fig. 10, it can be said that the ripple voltage in output is around 5 mV which is under the limit of 10 mV.

Current and voltage plots are shown in Fig. 11. The input circuit, consisting of nine solar cells and a filter capacitor (C1), has the capacity to deliver a maximum current of 5A. It is important to note that, like how voltage cannot instantaneously change across a capacitor, the current through the inductor does not make an instantaneous jump to 5A. As depicted in Fig. 11, when the voltage across the input filter capacitor C1 reaches 19.5V, the MPPT comparator activates the MOSFET, causing the current to start at 0A and gradually build up exponentially in the inductor. As the inductor's current increases, the voltage across capacitor C1 decreases exponentially. Once this voltage drops to 19V, the inductor's current reaches its maximum value of 5A. The speed at which the inductor goes from zero amperes to saturation depends on the specific inductor's value. The voltage decreases at the same rate that the current increases, following the voltage/current relationship of an inductor.

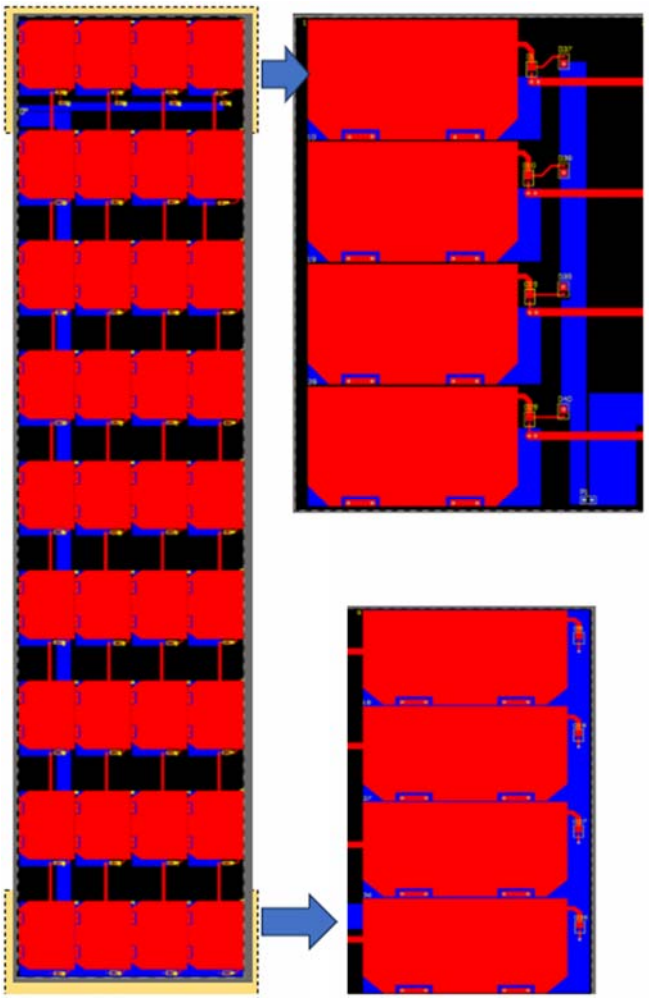

Fig. 8 Final PCB Layout

2) Thermal Analysis

The solar panel module has an embedded magnetorquer coil in four internal layers which acts as an attitude control system of the satellite [24]-[26]. Each layer has 6 coils and the four internal layers have a total of 24 coils. These coils can be connected in any arrangement (series, parallel or hybrid combination) which results in various amount of power consumption, torque generation and can increase the PCB surface temperature to different levels. In this session, various coil combinations are analyzed for the amount of power consumption and PCB surface temperature rise.

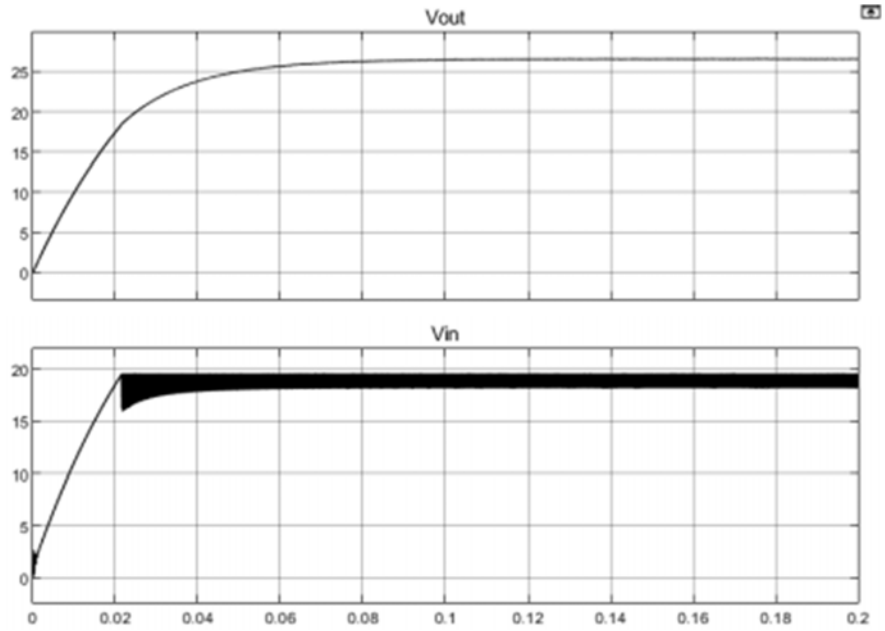

Fig. 9 Input and Output voltages of Boost Converter

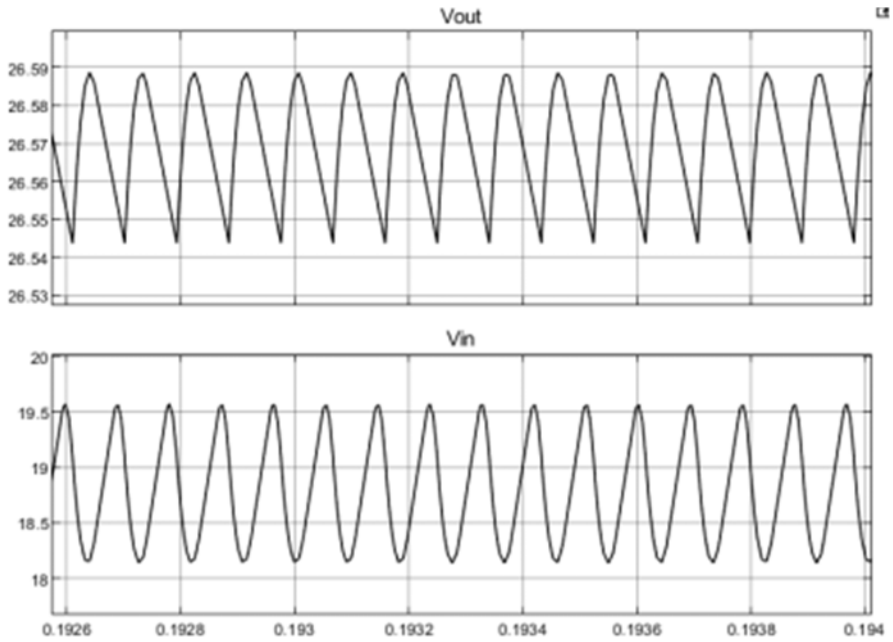

Fig. 10 Output voltage ripple of Boost Converter

- *Single coil:* Let start from the single coil analysis. A variable input voltage increasing from 0 ~ 28V is applied. This study revealed the coil's dynamic behavior, with a peak temperature of 30.2746 °C and a maximum current of 0.3325 Amp. The coil generated a maximum dissipated power of 9.31116 W.
- *Coils in series:* The setup displayed various responses as the voltage varied from 0 to 28 V, with a peak current of 0.01385 A. The behavior of the 24 coils connected in series was analyzed, and at a maximum temperature of 25.35 °C, the setup reached a maximum voltage of 1.16667 V. The setup generates a maximum power dissipation of 0.38765 W.
- *Coils in parallel:* As the voltage changed, the setup displayed various electrical behaviors and reached a maximum current of 0.498812 A. The highest temperature recorded was 109.051v°C. The setup produces a total power dissipation of 223.468 W during the voltage variation.
- *Coils in Combination of 4x6:* The setup reached a peak current of 0.2216 A. The maximum temperature recorded was 3.2747 °C. A maximum power dissipation of 13.9667 W was observed during the voltage change.

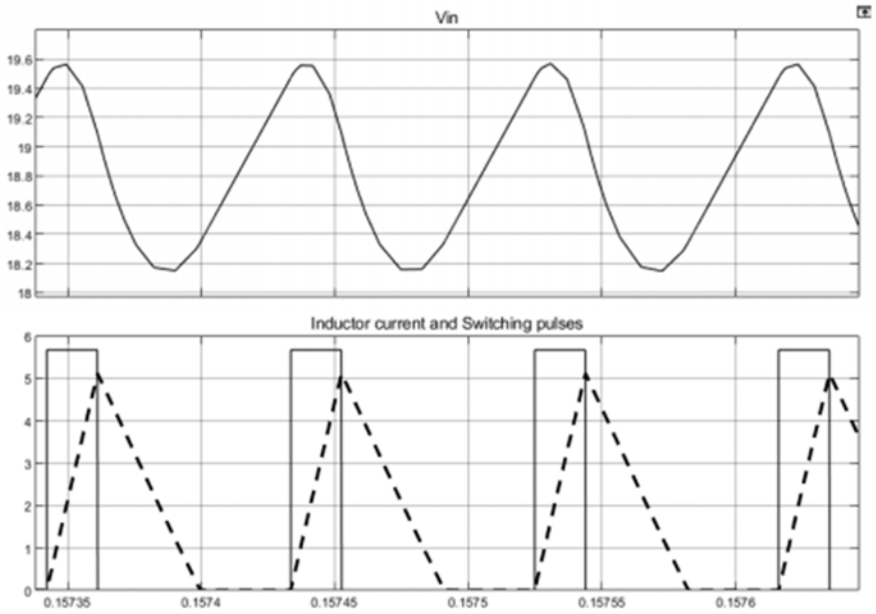

Fig. 11 Hysteresis graph of the Boost Converter

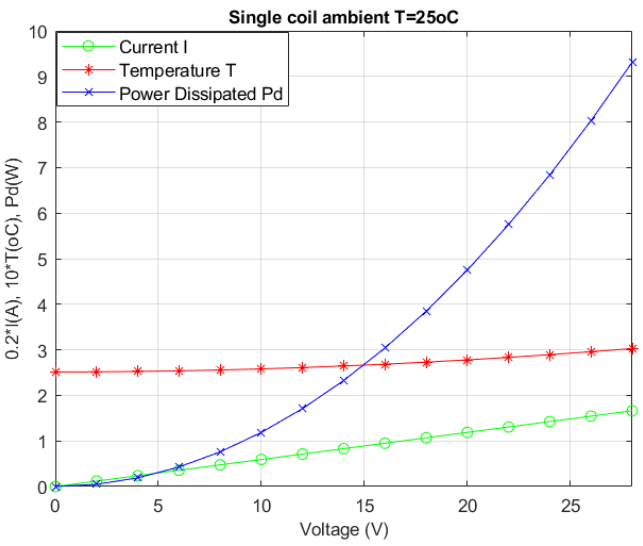

Fig. 12 I, T, Pd vs V graph for a single coil

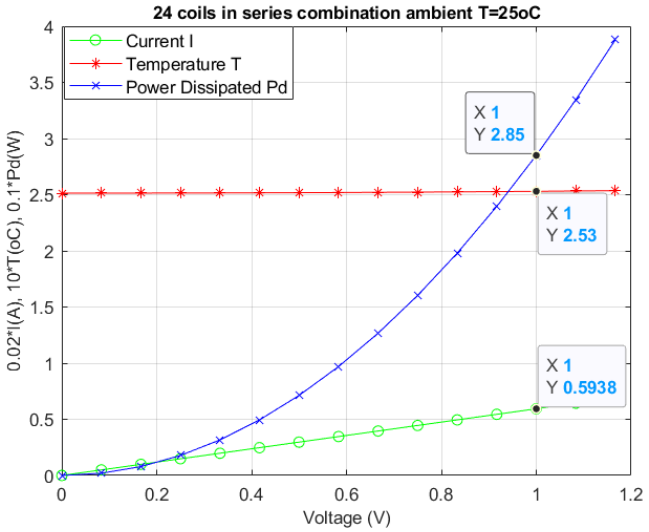

Fig. 13 I, T, Pd vs V graph for coils in series combination

- *Coils in Combination of 6x4:* The setup exhibited various electrical behaviors as the voltage varied, with a peak electrical current of 0.124 A. The setup reached a maximum temperature of 28.592 °C when the voltage ranged from 0 to 28V. With this setup, a maximum power dissipation of 6.20744 W generated during the voltage sweep.
- *Coils in Combination of 3x8:* The setup reached a peak electrical current of 0.8867 A. The maximum temperature recorded was 38.2937 °C. The setup required a maximum power dissipation of 24.829 W to avoid overheating and maintain safe operation.
- *Coils in Combination of 8x3:* As the voltage varied between 0 and 28V, the setup showed a peak electrical current of 0.124 A. The maximum temperature recorded was 27.0964 °C. The setup exhibits a maximum power dissipation of 3.49 W during the voltage sweep.
- *Coils in Combination of 2x12:* The setup reached a peak electrical current of 1.99525 A. The setup reached a maximum temperature of 52.6925 °C. The setup dissipates a maximum power of 55.867 W during the voltage change.
- *Coils in Combination of 12x2:* The setup displayed a peak current of 0.055423 A. The maximum temperature recorded was 26.0143 °C. The setup dissipates a maximum power dissipation of 1.55186 W during the voltage change.

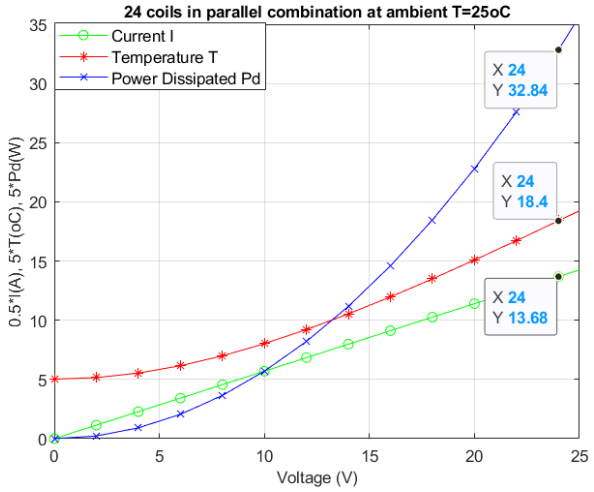

Fig. 14 I, T, Pd vs V graph for coils in parallel combination

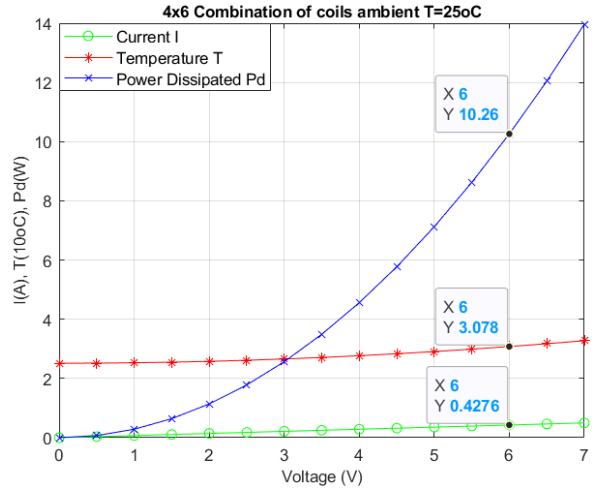

Fig. 15 I, T, Pd vs V graph for coils in 4X6 combination

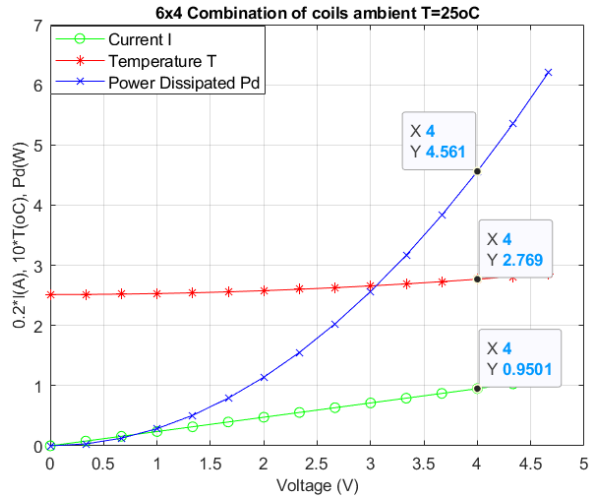

Fig. 16 I, T, Pd vs V graph for coils in 6X4 combination

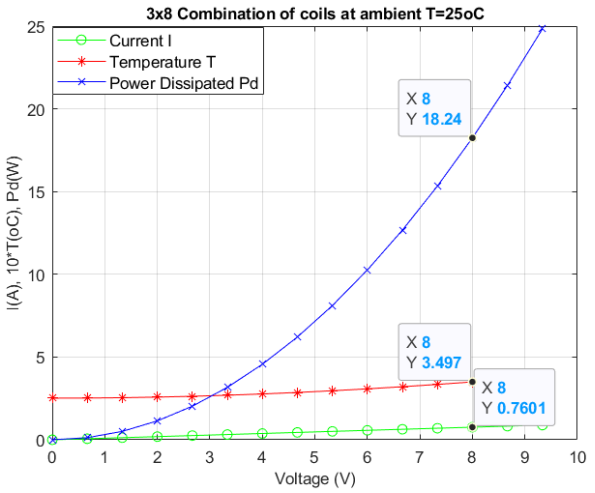

Fig. 17 I, T, Pd vs V graph for coils in 3X8 combination

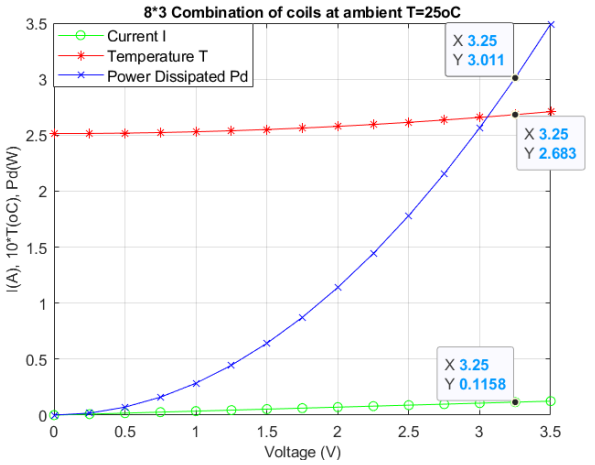

Fig. 18 I, T, Pd vs V graph for coils in 8X3 combination

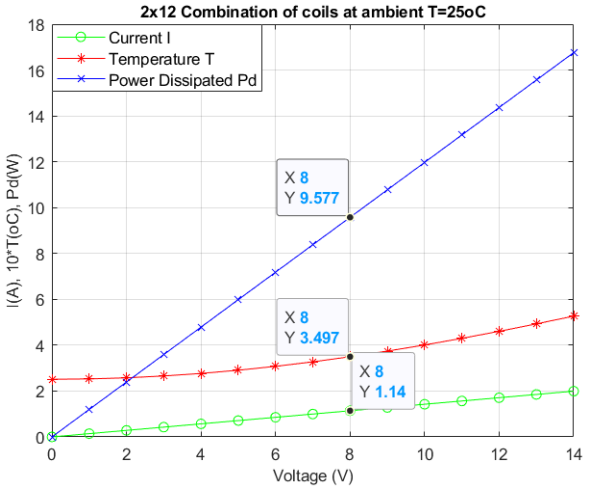

Fig. 19 I, T, Pd vs V graph for coils in 2X12 combination

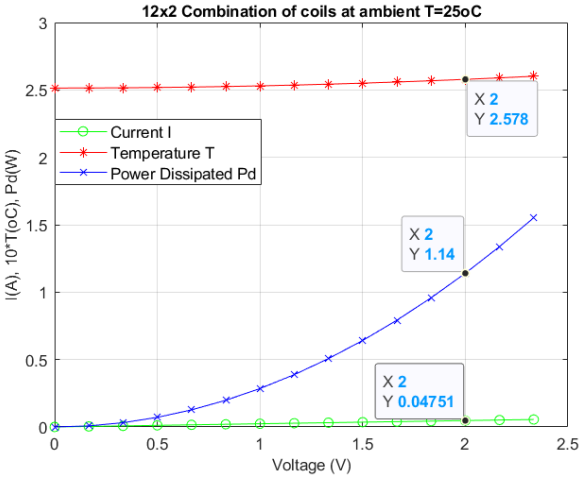

Fig. 20 I, T, Pd vs V graph for coils in 12X2 combination

V. Conclusion

Solar panel module along with an MPPT based boost converter was designed and analyzed for hexagonal shaped small satellite. The designed solar panel is composed of 36 solar cells with four parallel banks where each bank is composed of 9 solar cells. Solar panel output voltage is 19V whereas the power distribution bus (PDB) voltage is 28V. The output of solar panel (19V) has been successfully boosted 28V (PDB voltage level) using a boost converter with an output voltage ripple within the permissible limit (1%). The system has constant voltage MPPT technique which is created using a comparator hysteresis. The solar panel module also has an embedded magnetorquer coil in four internal layers. A thermal analysis was done at the end to analyze the temperature and power dissipated by the embedded magnetorquer coil. Various combinations of the coils are analyzed for power dissipation and respective PCB surface temperature rise. Thus, it was found that the PCB design can withstand all the energy dissipated thereby making this design a feasible one.

References

[1] Jakhu RS, Pelton JN. Small satellites and their regulation: Springer; 2014.
[2] Sandau R, Roeser H-P, Valenzuela A. Small satellite missions for earth observation. New Developments and Trends. 2010.
[3] Anwar Ali, Leonardo M. Reyneri, Juan Carlos de los Rios, Haider Ali, Innovative power management tile for NanoSatellites, in: Proceedings of the 63rd International Autronautical Congress, Naples, Italy, 1–5 October 2012
[4] M. U. Khan, A. Ali, H. Ali, M. S. Khattak and I. Ahmad, "Designing efficient Electric Power Supply System for Micro-Satellite," 2016 International Conference on Computing, Electronic and Electrical Engineering (ICE Cube), Quetta, Pakistan, 2016, pp. 207-212, doi: 10.1109/ICECUBE.2016.7495225.
[5] A. Ali, S. A. Khan, M. U. Khan, H. Ali, M. Rizwan Mughal, and J. Praks, "Design of modular power management and attitude control subsystems for a microsatellite," Int. J. Aerosp. Eng., vol. 2018, 2018, Art. no. 2515036.
[6] Reinhart RC, Kacpura TJ, Handler LM, Hall CS, Mortensen DJ, Johnson SK, et al. Space Telecommunications Radio System (STRS) Architecture Standard. Release 1.02. 1. 2012.
[7] Taylor J, Fernández MM, Bolea-Alamañac AI, Cheung KM. Deep Space 1. Deep Space Communications. 2016:135-92.
[8] Gilmore DG. Spacecraft Thermal Control Handbook, Fundamental Technologies, vol. I The Aerospace Press/American Institute of Aeronautics and Astronautics. Inc; 2002.
[9] Meseguer J, Pérez-Grande I, Sanz-Andrés A. Spacecraft thermal control: Elsevier; 2012.
[10] Bate RR, Mueller DD, White JE, Saylor WW. Fundamentals of astrodynamics: Courier Dover Publications; 2020.
[11] Ali MBOE, Abbaker AEM, Elfaki SEE, editors. Modeling, Simulation, and Implementation of the Electrical Power System of Cube Satellite Using Matlab and Simulink. 2020 International Conference on Computer, Control, Electrical, and Electronics Engineering (ICCCEEE); 2021: IEEE.
[12] ALBus hopes to increase power availability for CubeSats - NASA 2018, Available from: https://www.nasa.gov/general/albus-hopes-to-increase-power-availability-for-cubesats/.
[13] Popescu O. Power budgets for cubesat radios to support ground communications and inter-satellite links. IEEE Access. 2017;5:12618-25.
[14] Zhu F. 3.3 Payload Design. pressbooks-devoerhawaiiedu.
[15] Caldwell S. 7.0 Thermal Control 2021, Available from: https://www.nasa.gov/smallsat-institute/sst-soa/thermal-control/.
[16] Sher A, Baig MS, editors. Design and simulation of small satellite power system in Simulink/MATLAB for preliminary performance estimation. 2019 16th International Bhurban Conference on Applied Sciences and Technology (IBCAST); 2019: IEEE.
[17] Karagöz FE, İnce B, Şahin Y, Yıldırım D, Çetin E, Karahan M, et al., editors. Turkish First Indigenous 100V Satellite Power Subsystem. 2023 10th International Conference on Recent Advances in Air and Space Technologies (RAST); 2023: IEEE.
[18] Colasanti S, Nesswetter H, Zimmermann CG, Lugli P, editors. Modeling and parametric simulation of triple junction solar cell for space applications. 2014 IEEE 40th Photovoltaic Specialist Conference (PVSC); 2014: IEEE.
[19] Triple-Junction Solar Cell for Space Applications (CTJ30).
[20] Campesato R, Casale M, Gabetta G, Lisbona EF, D'Abrigeon L, editors. Thin and flexible triple junction cells 30% efficient: Qualification results and future space applications. 2017 IEEE 44th Photovoltaic Specialist Conference (PVSC); 2017: IEEE.
[21] Naveda-Castillo D, Adanaque-Infante L, editors. Characterization of DC converters for energy power systems on CubeSats. 2020 IEEE XXVII International Conference on Electronics, Electrical Engineering and Computing (INTERCON); 2020: IEEE.
[22] HIITIO, Solar Power Optimizer Manufacturer, https://www.hiitio.com/solar-power-optimizer-manufacturer/
[23] Hart DW. Power Electronics: Mcgraw-Hill; 2011.
[24] M. R. Mughal, H. Ali, A. Ali, J. Praks and L. M. Reyneri, "Optimized Design and Thermal Analysis of Printed Magnetorquer for Attitude Control of Reconfigurable Nanosatellites," in IEEE Transactions on Aerospace and Electronic Systems, vol. 56, no. 1, pp. 736-747, Feb. 2020, doi: 10.1109/TAES.2019.2933959.
[25] Ali A, Khan SA, Dildar MA, Ali H, Ullah N (2018) Design & thermal modeling of solar panel module with embedded reconfigurable Air-Coil for micro-satellites. PLoS ONE 13(7): e0199145. https://doi.org/10.1371/journal.pone.0199145
[26] A. Ali, M. R. Mughal, H. Ali, L. M. Reyneri and M. N. Aman, "Design, implementation, and thermal modeling of embedded reconfigurable magnetorquer system for nanosatellites," in IEEE Transactions on Aerospace and Electronic Systems, vol. 51, no. 4, pp. 2669-2679, Oct. 2015, doi: 10.1109/TAES.2015.130621.